PAPER

Spatial magnetization profile in spherical nanomagnets with surface anisotropy: Green's function approach

To cite this article: M P Adams *et al* 2023 *Phys. Scr.* **98** 105512

Physica Scripta

PAPER

Spatial magnetization profile in spherical nanomagnets with surface anisotropy: Green's function approach

M P Adams[1], **A Michels**[1] **and H Kachkachi**[2,*]

[1] Department of Physics and Materials Science, University of Luxembourg, 162A avenue de la Faiencerie, L-1511 Luxembourg, Grand Duchy of Luxembourg, Luxembourg
[2] Université de Perpignan via Domitia, Lab. PROMES CNRS UPR8521, Rambla de la Thermodynamique, Tecnosud, 66100 Perpignan, France
[*] Author to whom any correspondence should be addressed.

E-mail: michael.adams@uni.lu, andreas.michels@uni.lu and hamid.kachkachi@univ-perp.fr

Abstract

We consider a single spherical nanomagnet and investigate the spatial magnetization profile $\mathbf{m}(\mathbf{r})$ in the continuum approach, using the Green's function formalism. The energy of the (many-spin) nanomagnet comprises an isotropic exchange interaction, a uniaxial anisotropy in the core and Néel's surface anisotropy, and an external magnetic field. We derive a semi-analytical expression for the magnetization vector field $\mathbf{m}(\mathbf{r})$ for an arbitrary position $\mathbf{r}$ within and on the boundary of the nanomagnet, as a solution of a homogeneous Helmholtz equation with inhomogeneous Neumann boundary conditions. In the absence of core anisotropy, we use the solution of this boundary problem and infer approximate analytical expressions for the components m_α, $\alpha = x, y, z$, as a function of the radial distance r and the direction solid angle. Then, we study the effects of the nanomagnet's size and surface anisotropy on the spatial behavior of the net magnetic moment. In the presence of a core anisotropy, an approximate analytical solution is only available for a position $\mathbf{r}$ located on the surface, i.e. $\mathbf{r} = R\mathbf{n}$, where R is the radius of the nanomagnet and $\mathbf{n}$ the verse of the normal to the surface. This solution yields the maximum spin deviation as a result of the competition between the uniaxial core anisotropy and Néel's surface anisotropy. Along with these (semi-)analytical calculations, we have solved a system of coupled Landau–Lifshitz equations written for the atomic spins, and compared the results with the Green's function approach. For a plausible comparison with experiments, e.g. using the technique of small-angle magnetic neutron scattering, we have averaged over the direction solid angle and derived the spatial profile in terms of the distance r. We believe that the predictions of the present study could help to characterize and understand the effects of size and surface anisotropy on the magnetization configurations in nanomagnet assemblies such as arrays of well-spaced platelets.

1. Introduction

Why has studying nanoscaled systems suddenly become so important? How can a material that is so small be so influential as to trigger a tremendous research activity worldwide? To understand the power of nanomaterials, we need to understand how materials work at the very small scale. When the dimensions of the system are reduced down to the nanoscale, the first big change is the larger proportion of atoms at its surface, and this leads to a dramatic change in the chemical and physical properties. For example, bulk gold is an inert metal that does not react much and thus does not rust, whereas at the nanoscale, it works as a catalyst. A nanoparticle of gold about 90 nm in size absorbs red and yellow light from the color spectrum, making the nanoparticle appear blue or green [1]. However, the same nanoparticle that is only 30 nm in size, absorbs blue and green light, and so appears red. Today, we know that this is so because the optical properties of metal nanoparticles are dominated by the surface plasmon resonances for both absorption and scattering of light [2]. At the bottom end of the nanoscale, quantum phenomena start to emerge through a transition from the electronic-band structure to

discrete energy levels [3]. This fundamentally alters the material properties and leads to many new phenomena [4], such as the energy gap and excitonic absorption of light, unique catalytic activity, and single-electron magnetism. In addition to the electronic structure alteration, the crystal structure also starts to exhibit significant changes with respect to the bulk material.

The reduction of the size and the entailed changes in the electronic and crystal structure fundamentally alter the magnetic properties as well. As the size reduces to the nanometer, the magnetic system, nowadays called *a nanomagnet*, exhibits a new phenomenon known as *superparamagnetism* [5, 6] with a change in the relevant temperature by an order of magnitude and in the relaxation time by several orders of magnitude. Furthermore, the large surface contribution in nanoscaled magnetic systems leads to inhomogeneous atomic-spin configurations [see [7–11] and references therein] and thereby to a drastically different behavior in response to external stimuli. For example, new modes of magnetization switching play a crucial role in many new spintronic applications [12]. Likewise, these surface-induced effects strongly affect the relaxation processes owing to a more complex potential energy and new excitation modes [13, 14].

Therefore, in order to understand and master the new magnetic properties of nano-elements, in view of efficient practical applications, it is essential to probe the novel features induced by their surfaces and interfaces. In particular, it is crucial to investigate the atomic-spin configurations within the nanomagnets and characterize the spatial profile of their magnetization. In this work, we present a study of the latter within spherical nanomagnets using the technique of Green's functions (GF). This is part of a broader work that makes use of complementary techniques with the aim to better characterize surface-induced spin noncollineartities and their effects on the equilibrium and dynamic behaviors of assemblies of nanomagnets. In this context, the present work provides a general formalism that renders fairly precise and useful analytical expressions of the spatial magnetization profile, clearly presenting all the involved mathematical steps and approximations. As a byproduct, it confirms and elaborates on the conclusions reached by previous works regarding the effects of surface anisotropy in nanomagnets.

When averaged over the solid angle, the spatial magnetization profile may be compared with experiments, such as magnetic small-angle neutron scattering (SANS)[15] in assemblies of nanomagnets. Indeed, the present formalism constitutes a basis for computing the magnetic SANS cross-section of nanomagnets as a function of their various physical parameters. Accordingly, in a recent study [16, 17], we investigated the signature of surface-induced spin misalignments in the SANS cross section upon varying the applied magnetic field and the nanomagnet energy parameters.

Plan of the article: After an introduction, in section 2, we present our model for a nanomagnet, viewed as a crystallite of $\mathcal{N}$ atomic magnetic moments and then describe the continuum approach for studying the spatial profile of its magnetization. In section 3, we use the Green's function technique to obtain the spin deviation vector in terms of surface anisotropy, in addition to other parameters, both with and without the anisotropy in the core. We plot the magnetization profile in the radial direction and study its behavior as we vary the size of the nanomagnet and the anisotropy constants. The results from the Green's function formalism are also compared to the numerical calculations based on the solution of the system of coupled Landau–Lifshitz equations. Finally, in section 4, we summarize the main results of this work and discuss the possibility of experimentally investigating the surface-induced spin-misalignments, e.g. by SANS technique. The paper ends with an Appendix.

2. Many-spin nanomagnet

2.1. Discrete lattice

A many-spin nanomagnet (NM) is viewed as a crystallite of $\mathcal{N}$ atomic magnetic moments $\boldsymbol{\mu}_i = \mu_a \mathbf{m}_i$ ($\|\mathbf{m}_i\| = 1$) with $\mu_a = M_s v_0$, where M_s is the saturation magnetization and v_0 is the volume of the unit cell of the underlying lattice. The magnetic state of the NM may be investigated with the help of the atomistic approach based on the anisotropic (classical) Dirac-Heisenberg Hamiltonian [7, 18–25]

$$
\begin{aligned}
\mathcal{H} &= -\frac{1}{2}\sum_{\langle i,j \rangle} J_{ij}\, \mathbf{m}_i \cdot \mathbf{m}_j - \mu_a \mathbf{H}_{\text{ext}} \cdot \sum_{i=1}^{\mathcal{N}} \mathbf{m}_i + \sum_{i=1}^{\mathcal{N}} \mathcal{H}_{\text{an},i} \\
&\equiv \mathcal{H}_{\text{exc}} + \mathcal{H}_{\text{Z}} + \mathcal{H}_{\text{an}},
\end{aligned}
\tag{1}
$$

where $\mathcal{H}_{\text{exc}}$ is the (nearest-neighbor) exchange energy, $\mathcal{H}_{\text{Z}}$ the Zeeman contribution and $\mathcal{H}_{\text{an}} \equiv \sum_{i=1}^{\mathcal{N}} \mathcal{H}_{\text{an},i}$ the anisotropy energy with $\mathcal{H}_{\text{an},i} = -K_i\, \mathcal{A}(\mathbf{m}_i)$, being the anisotropy contribution of each spin on site i; $\mathcal{A}(\mathbf{m}_i)$ is the anisotropy function that depends on the locus of the atomic spin $\mathbf{s}_i$. So, for core spins, the anisotropy may be uniaxial and/or cubic, while for surface spins there are a few models for on-site anisotropy that is very often taken as uniaxial with either a transverse or parallel easy axis. There is also the more plausible model proposed by Néel [26] for which $\mathcal{A}(\mathbf{m}_i) = \frac{1}{2}\sum_{j=1}^{z_i}(\mathbf{m}_i \cdot \mathbf{u}_{ij})^2$, where z_i is the coordination number at site i and $\mathbf{u}_{ij}$ a unit
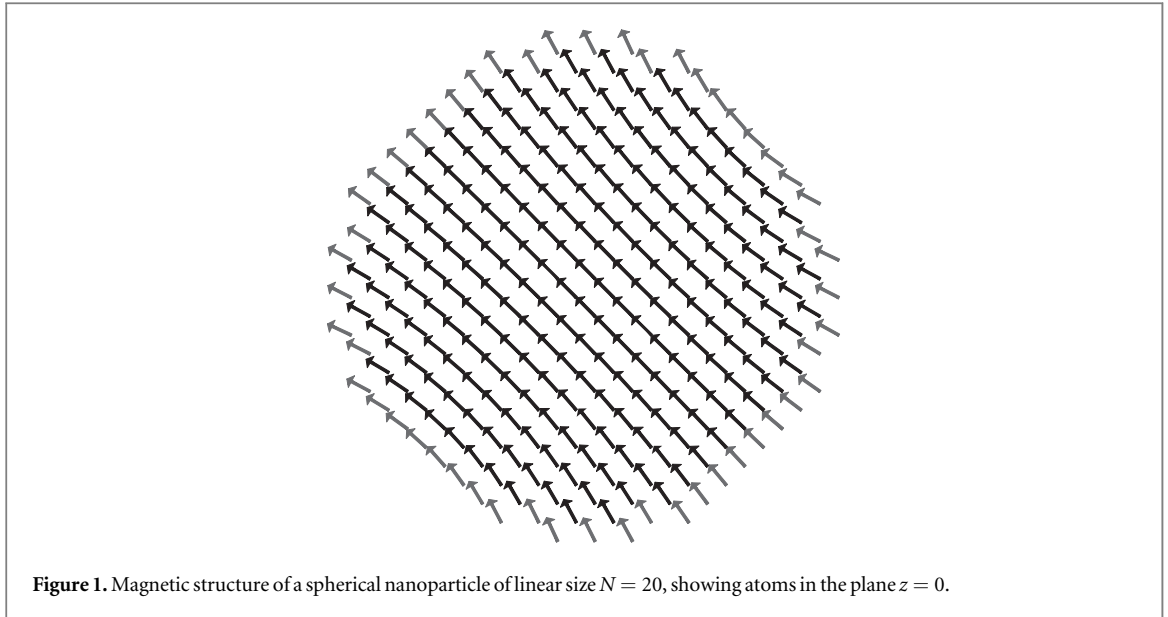
Figure 1. Magnetic structure of a spherical nanoparticle of linear size $N = 20$, showing atoms in the plane $z = 0$.

vector connecting the nearest neighbors i, j. The constant $K_i > 0$ is usually denoted by K_c if the site i is in the core and by K_s if it is on the boundary.

Therefore, in the sequel we will refer to the Néel Surface Anisotropy (NSA) model and this means that we consider a uniaxial anisotropy in the core with easy axis (whose verse is the unit vector $\mathbf{e}_A$) and Néel's on-site anisotropy for spins on the surface. More precisely, in the NSA model we adopt the following anisotropy energy

$$\mathcal{H}_{\mathrm{an},i} = \begin{cases} -K_c (\mathbf{m}_i \cdot \mathbf{e}_A)^2, & i \in \text{core} \\ +\dfrac{1}{2} K_s \displaystyle\sum_{j \in \mathrm{n.n.}} (\mathbf{m}_i \cdot \mathbf{u}_{ij})^2, & i \in \text{surface}. \end{cases} \tag{2}$$

The macroscopic state of the NM may be described using what is often called the *superspin* or *macrospin*, that is the net magnetic moment

$$\mathbf{m} = \frac{1}{\mathcal{N}} \sum_{i=1}^{\mathcal{N}} \mathbf{m}_i. \tag{3}$$

The dynamics of the magnetic moments $\mathbf{m}_i$ is governed by the (damped) Landau–Lifshitz equation (LLE) or, more precisely, the system of coupled Landau–Lifshitz equations written for the atomic magnetic moments $\mathbf{m}_i$ ($i = 1, 2, \ldots, \mathcal{N}$),

$$\frac{d\mathbf{m}_i}{d\tau} = \mathbf{m}_i \times \mathbf{h}_{\mathrm{eff},i} - \alpha \mathbf{m}_i \times (\mathbf{m}_i \times \mathbf{h}_{\mathrm{eff},i}), \tag{4}$$

with the (normalized) local effective field $\mathbf{h}_{\mathrm{eff},i}$, acting on $\mathbf{s}_i$, being defined by $\mathbf{h}_{\mathrm{eff},i} = -\delta\mathcal{H}/\delta\mathbf{s}_i$. τ is the reduced time given by $\tau = t/\tau_s$, where $\tau_s = \mu_a/(\gamma J)$ is a characteristic time of the system's dynamics; $\gamma \simeq 1.76 \times 10^{11}$ (Ts)$^{-1}$ is the gyromagnetic ratio and α the damping parameter ($\sim 0.01 - 0.1$). For example, for cobalt $J = 8$ meV and $\tau_s = 70$ fs. In these units, $\mathbf{h}_{\mathrm{eff},i} = \mu_a \mathbf{H}_{\mathrm{eff},i}/J$, where $\mathbf{H}_i^{\mathrm{eff}} = -(1/\mu_a)(\delta\mathcal{H}/\delta\mathbf{m}_i)$ is the deterministic field that comprises the exchange field, the magnetic field $\mathbf{H}_{\mathrm{ext}}$ and the anisotropy field $\mathbf{H}_A$.

The spin configuration shown in figure 1, with the net magnetic moment along the diagonal, is obtained by (numerically) minimizing the energy (1) by solving the system of coupled Landau–Lifshitz equations (4) [7, 23, 27–30]. This is a typical spin structure that is induced by the NSA in a spherical NM. Note that the atomic magnetic moments $\mathbf{m}_i$ progressively deviate from the global orientation (here the diagonal) as the site i is located closer to the NM border and away from the diagonal.

Orders of magnitude of materials parameters: Let us now give a few orders of magnitude of the physical parameters that appear in the Hamiltonian (1). First of all, we note that equation (1) is the energy per atom, obtained by dividing the total energy of the system by $\mathcal{N}$, the number of atoms in the NM. Hence, the physical parameters involved, namely J, K and $\mu_a(\mu_0 H)$, are measured in Joule per atom. For instance, the anisotropy energy, which is often written as $\tilde{K}V$ where V is the volume of the NM and $\tilde{K}$ the density of anisotropy energy (in J/m³), becomes $\tilde{K}V = \mathcal{N}v_0\tilde{K} \equiv \mathcal{N}K$. Similarly, the Zeeman contribution which usually reads $\mu_0 HM$ is now

rewritten as $\mu_0 H M = \mathcal{N} \mu_a (\mu_0 H)$.[3] In the NSA model, we distinguish between the core (full coordination) and surface atoms (with smaller coordination). As such, the anisotropy constant K_c applies only to atoms in the core of the NM and K_s only to those on its surface. For instance, for cobalt, the magnetic moment per atom $\mu_a = n_0 \mu_B$, with n_0 being the number of Bohr magnetons per atom ($n_0 \simeq 1.7$) and $\mu_B = 9.274 \times 10^{-24}$ J/T is the Bohr magneton. Hence, $\mu_a \simeq 1.58 \times 10^{-23}$ J/T. Next, the magneto-crystalline anisotropy constant is roughly $K_c \simeq 3 \times 10^{-24}$ J/atom, the surface anisotropy constant is around $K_s \simeq 5.22 \times 10^{-23}$ Joule/atom and the (bulk) exchange coupling is $J \simeq 8$ mev or 1.2834×10^{-21} J/atom. The lattice parameter is $a=0.3554$nm. As such, $k_c \equiv K_c/J \simeq 0.00234$ while $k_s \equiv K_s/J \simeq 0.04$. The latter value is within the range of values estimated by several experimental studies. Indeed, one may find $K_s/J \simeq 0.1$ for cobalt [31], $K_s/J \simeq 0.06$ for iron [32], and $K_s/J \simeq 0.04$ for maghemite particles [33].

2.2. Continuum approach

In the continuum approach, the magnetic configuration of a system is described by the continuous magnetization vector field $\mathbf{M}(\mathbf{r})$ constrained to a constant norm M_s. The relation between the discrete and continuous descriptions is [34]

$$\mathbf{M}(\mathbf{r}) = \sum_i \boldsymbol{\mu}_i \Big/ v_0 \tag{5}$$

where $\boldsymbol{\mu}_i$ is the discrete magnetic moment of the ith ion belonging to a given sub-lattice. The summation is carried over all sites in a physically small volume v_0, around a point whose position is $\mathbf{r} = (x, y, z)$, and within which the moments $\boldsymbol{\mu}_i$ are assumed to be uniform. The normalized magnetization density vector field is then defined by

$$\mathbf{m}(\mathbf{r}) \equiv \mathbf{M}(\mathbf{r})/M_s. \tag{6}$$

In the continuum limit, the exchange interaction is written in terms of the exchange stiffness A (e.g. about 3.6 pJ/m for cobalt) as an integral over the volume V of the NM

$$\mathcal{H}_{\text{exc}} = A \int_V d\mathbf{r} \sum_{\alpha=x,y,z} (\boldsymbol{\nabla} m_\alpha \cdot \boldsymbol{\nabla} m_\alpha). \tag{7}$$

For a simple cubic lattice, we have the relation between J and A: $A = J/2a$, with a being the lattice constant. This is the classical analog of the relation that applies to a simple cubic lattice of quantum spins, $A = J \langle S^2 \rangle /2a$.

Using the identity $\nabla \cdot (m_\alpha \cdot \nabla m_\alpha) = m_\alpha \Delta m_\alpha + (\nabla m_\alpha)^2$ and the divergence theorem, the exchange energy can split into a core and a surface contribution, namely

$$\mathcal{H}_{\text{exc}} = -A \sum_{\alpha=x,y,z} \int_V m_\alpha \Delta m_\alpha \, d^3 r + A \sum_{\alpha=x,y,z} \oint_{\partial V} m_\alpha \nabla m_\alpha \, \mathbf{n} \, d^2 r. \tag{8}$$

Next, the Zeeman term reads,

$$\mathcal{H}_{\text{Z}} = -M_s \mathbf{H}_{\text{ext}} \cdot \int_V d^3 r \, \mathbf{m}(\mathbf{r}) \tag{9}$$

and the anisotropy energy for core spins becomes

$$\mathcal{H}_{\text{core}} = -\frac{K_c}{v_0} \int_{V_{\text{in}}} d^3 r (\mathbf{m} \cdot \mathbf{e}_z)^2.$$

Note that V_{in}/v_0, with $v_0 = a^3$, is equal to the number of core atoms that we denote by N_c, so that $V_{\text{in}} K_c/v_0 = N_c K_c$. Regarding surface anisotropy, it was shown in [27] that the corresponding energy in the NSA model can be replaced by the approximate expression for a sphere [see [35] for a cube]

$$\mathcal{H}_{\text{surface}} = -\frac{K_s}{2} \sum_\alpha |n_\alpha| \, m_\alpha^2, \tag{10}$$

where $\mathbf{n}$ is the unit vector of the normal to the surface (the boundary ∂V of the NM). Then, in the continuum limit, $\mathcal{H}_{\text{surface}}$ becomes

$$\mathcal{H}_{\text{surface}} = -\frac{K_s}{2a^2} \sum_{\alpha=x,y,z} \oint_{\partial V} d^2 r |n_\alpha| \, m_\alpha^2.$$

Therefore, collecting all contributions, the nanomagnet's Hamiltonian in equation (1) becomes in the continuum approach

---

[3] The magnetic field H in (1), and all subsequent equations, should be understood as $\mu_0 H$ which is measured in Tesla, so that the Zeeman term $\mu_a (\mu_0 H)$ is measured in J/atom.

$$\mathcal{H} = A \sum_{\alpha \in \{x,y,z\}} \left[\oint_{\partial V} m_\alpha \boldsymbol{\nabla} m_\alpha \cdot \mathbf{n} \, d^2 r - \int_V m_\alpha \Delta m_\alpha \, d^3 r \right]$$
$$- M_s \mathbf{H}_{\text{ext}} \cdot \int_V d^3 r \, \mathbf{m}(\mathbf{r})$$
$$- \frac{K_c}{a^3} \int_V (\mathbf{m} \cdot \mathbf{e}_A)^2 \, d^3 r - \frac{K_s}{2a^2} \sum_{\alpha \in \{x,y,z\}} \oint_{\partial V} |n_\alpha| \, m_\alpha^2 \, d^2 r. \tag{11}$$

In the case of small spin-misalignment, where the magnetization density $\mathbf{m}(\mathbf{r})$ slightly deviates from the homogeneous magnetization state $\mathbf{m}_0$ [see figure 1], a perturbation approach is applicable. Accordingly, $\mathbf{m}_0$ is considered as the principal unit vector[4] associated with $\mathbf{m}(\mathbf{r})$ while the spin-misalignment is encoded in the vector field $\boldsymbol{\psi}(\mathbf{r})$ with $\boldsymbol{\psi}(\mathbf{r}) \perp \mathbf{m}_0$. Therefore, we write [36, 37]

$$\mathbf{m}(\mathbf{r}) = \mathbf{m}_0 \sqrt{1 - \|\boldsymbol{\psi}(\mathbf{r})\|^2} + \boldsymbol{\psi}(\mathbf{r}), \tag{12}$$

with $\mathbf{m}_0 \cdot \boldsymbol{\psi} = 0$ and thereby $|\mathbf{m}(\mathbf{r})| = 1$, together with the condition (discussed later in the text)

$$\int_V d^3 r \, \boldsymbol{\psi}(\mathbf{r}) = 0. \tag{13}$$

Assuming that $\psi_\alpha \ll 1, \alpha = x, y, z$, an approximate closed-form solution for the normalized magnetization density can be obtained by performing the second-order expansion of equation equation (12) with respect to $\boldsymbol{\psi}$:

$$\mathbf{m}(\mathbf{r}) \cong \mathbf{m}_0 + \boldsymbol{\psi}(\mathbf{r}) - \frac{1}{2} \|\boldsymbol{\psi}(\mathbf{r})\|^2 \mathbf{m}_0. \tag{14}$$

Next, one can rewrite the Hamiltonian (11) using a perturbation approach and minimizing with respect to the Cartesian components ψ_x, ψ_y, ψ_z, leading to a homogeneous (vector) Helmholtz equation for these components, together with inhomogeneous Neumann boundary conditions. However, owing to the transverse character of $\boldsymbol{\psi}$ ($\mathbf{m}_0 \cdot \boldsymbol{\psi} = 0$), it is more convenient to work in the local frame attached to $\mathbf{m}_0$, i.e. $(\mathbf{m}_0, \mathbf{u}_1, \mathbf{u}_2)$, where $\mathbf{u}_1$ and $\mathbf{u}_2$ are the following two unit vectors [37]

$$\mathbf{u}_1 = \frac{\mathbf{m}_0 \times \mathbf{e}_A}{\|\mathbf{m}_0 \times \mathbf{e}_A\|}, \quad \mathbf{u}_2 = \frac{\mathbf{m}_0(\mathbf{m}_0 \cdot \mathbf{e}_A) - \mathbf{e}_A}{\|\mathbf{m}_0(\mathbf{m}_0 \cdot \mathbf{e}_A) - \mathbf{e}_A\|}. \tag{15}$$

In the new frame, we have

$$\boldsymbol{\psi} = \psi_1 \mathbf{u}_1 + \psi_2 \mathbf{u}_2 \tag{16}$$

and $\|\boldsymbol{\psi}(\mathbf{r})\|^2 = \psi_1^2 + \psi_2^2$. Consequently, with the help of a linear transformation, the problem is readily reduced to the following system of decoupled homogeneous scalar (dimensionless) Helmholtz equations

$$[\Delta_\xi - \kappa_\beta^2] \psi_\beta(\boldsymbol{\xi}) = 0, \quad \beta = 1, 2 \tag{17}$$

along with the inhomogeneous Neumann boundary conditions

$$\left. \frac{d\psi_\beta}{d\xi} \right|_{\xi=1} = \tilde{k}_s \sum_{\alpha=x,y,z} |n_\alpha| (\mathbf{m}_0 \cdot \mathbf{e}_\alpha)(\mathbf{u}_\beta \cdot \mathbf{e}_\alpha), \quad \beta = 1, 2. \tag{18}$$

Here we have introduced the dimensionless coordinates $\boldsymbol{\xi} = \mathbf{r}/R$, where R is the NM radius, together with the following Helmholtz coefficients $\kappa_\beta, \beta = 1, 2$, given by

$$\begin{cases} \kappa_1^2 = (\tilde{\mathbf{h}}_{\text{ext}} \cdot \mathbf{m}_0) + 2\tilde{k}_c \cdot (\mathbf{m}_0 \cdot \mathbf{e}_A)^2, \\ \kappa_2^2 = (\tilde{\mathbf{h}}_{\text{ext}} \cdot \mathbf{m}_0) + 2\tilde{k}_c \cdot [2(\mathbf{m}_0 \cdot \mathbf{e}_A)^2 - 1]. \end{cases} \tag{19}$$

where

$$\tilde{k}_c = \frac{1}{2} \left(\frac{D}{a}\right)^2 k_c, \qquad \tilde{k}_s = \left(\frac{D}{a}\right) k_s, \qquad \tilde{h}_{\text{ext}} = \frac{1}{2} \left(\frac{D}{a}\right)^2 h_{\text{ext}}, \tag{20}$$

with $D = 2R$ being the diameter of the NM, $k_c \equiv K_c/J$ and $k_s \equiv K_s/J$ the (dimensionless) reduced anisotropy constants introduced earlier, and $h_{\text{ext}} \equiv \mu_a H_{\text{ext}}/J$ the reduced magnetic field.

For later use and simplicity of notation, we introduce the surface anisotropy field

$$\Sigma_\beta(\mathbf{m}_0, \mathbf{n}) \equiv \left. \frac{d\psi_\beta}{d\xi} \right|_{\xi=1}. \tag{21}$$

---

[4] In all subsequent formulae, $\mathbf{m}_0$ is considered as a known uniform vector field.

In the case of a core anisotropy easy axis in the z direction, $\mathbf{e}_A = \mathbf{e}_z$,

$$\mathbf{u}_1 = \frac{\mathbf{m}_0 \times \mathbf{e}_z}{\sqrt{1 - m_{0,z}^2}}, \qquad \mathbf{u}_2 = \frac{\mathbf{m}_0(\mathbf{m}_0 \cdot \mathbf{e}_z) - \mathbf{e}_z}{\sqrt{1 - m_{0,z}^2}}, \tag{22}$$

and

$$\Sigma_1 = \tilde{k}_s \frac{m_{0,x} m_{0,y}}{\sqrt{1 - m_{0,z}^2}}(|n_x| - |n_y|),$$

$$\Sigma_2 = \tilde{k}_s \frac{m_{0,z}}{\sqrt{1 - m_{0,z}^2}}[(|n_x| - |n_z|)m_{0,x}^2 + (|n_y| - |n_z|)m_{0,y}^2]. \tag{23}$$

3. Magnetization profile: Green's function approach

To solve the homogeneous Helmholtz equation (17) for ψ_β, with the inhomogeneous Neumann boundary conditions (18), a specified gradient on the surface, we use the Green's function (GF) approach [38–40]. The GF $\mathcal{G}_\beta(\boldsymbol{\xi}, \boldsymbol{\xi}')$ for this problem satisfies the equation

$$[\Delta_\xi - \kappa_\beta^2]\mathcal{G}_\beta(\boldsymbol{\xi}, \boldsymbol{\xi}') = -4\pi\delta(\boldsymbol{\xi} - \boldsymbol{\xi}'), \tag{24}$$

and may be chosen to satisfy the homogeneous boundary condition of the same type as ψ_β, i.e. Neumann boundary conditions,

$$\left.\frac{d\mathcal{G}_\beta}{d\xi}\right|_{\xi=1} = 0. \tag{25}$$

In this case, we have the solution [27, 38–40]

$$\psi_\beta(\boldsymbol{\xi}) = \frac{1}{4\pi}\oint_{\partial V} d^2n' \, \Sigma_\beta(\mathbf{m}_0, \mathbf{n}')\mathcal{G}_\beta(\boldsymbol{\xi}, \mathbf{n}') \tag{26}$$

for $\boldsymbol{\xi}$ inside and on its boundary ∂V, where $\Sigma_\beta(\mathbf{m}_0, \mathbf{n}) = \left.\frac{d\psi_\beta}{d\xi}\right|_{\xi=\mathbf{n}} = (\boldsymbol{\nabla}_\xi \psi_\beta) \cdot \mathbf{n}$ is the outward normal gradient of ψ_β at the surface of the NM, with $\mathbf{n} = (\sin\theta\cos\varphi, \sin\theta\sin\varphi, \cos\theta)$ and $d^2n = d\Omega = \sin\theta \, d\theta d\varphi$.

The result in equation (26) simply reflects the fact that the source of spin mis-alignment ψ_β within the NM spin configuration is induced by surface anisotropy via the field $\Sigma_\beta = \left.\frac{d\psi_\beta}{d\xi}\right|_{\xi=\mathbf{n}}$ given in equation (18). As discussed in [27], the spin mis-alignment (or disorder) initiated at the surface of the NM propagates into the body of the latter down to its center. In this case, the contribution of surface anisotropy to the overall anisotropy of the NM scales with its volume (N^3). In the presence of uniaxial anisotropy in the core, the surface spin disorder is screened out at a certain distance from the center and the contribution of the surface to the overall anisotropy then scales as the surface (N^2) [see section 3.2 for further discussion].

3.1. No core anisotropy

In the absence of core anisotropy ($K_c = 0$) and magnetic field, $\kappa_1^2 = \kappa_2^2 = 0$ (see equation (19)), the vector $\mathbf{m}_0$ is along the cube diagonal, i.e. $m_{0,\alpha} = 1/\sqrt{3}$. Then, equation (17) reduces to the Laplace equation $\Delta\psi_\beta = 0$, subjected again to the inhomogeneous Neumann boundary conditions (18). The corresponding GF $\mathcal{G}^{(0)}(\boldsymbol{\xi}, \boldsymbol{\xi}')$ satisfies the Poisson equation

$$\Delta\mathcal{G}^{(0)}(\boldsymbol{\xi}, \boldsymbol{\xi}') = -4\pi\delta(\boldsymbol{\xi} - \boldsymbol{\xi}'). \tag{27}$$

However, integrating over the volume of the NM, we can see that the homogeneous boundary condition (25) can no longer be used. Instead, setting $\left.\frac{d\mathcal{G}_\beta}{d\xi}\right|_{\xi=1} = C$, i.e. an inhomogeneous Neumann boundary condition, one finds that $C = -1$, and the GF function of the problem is then given by [27, 41] (up to a constant)

$$\mathcal{G}^{(0)}(\boldsymbol{\xi}, \boldsymbol{\xi}') = \frac{1}{|\boldsymbol{\xi} - \boldsymbol{\xi}'|} + \frac{1}{\sqrt{1 + \xi^2\xi'^2 - 2(\boldsymbol{\xi} \cdot \boldsymbol{\xi}')}}$$

$$- \ln|1 - (\boldsymbol{\xi} \cdot \boldsymbol{\xi}') + \sqrt{1 + \xi^2\xi'^2 - 2(\boldsymbol{\xi} \cdot \boldsymbol{\xi}')}|. \tag{28}$$

$$\left.\frac{d\mathcal{G}^{(0)}}{d\xi}\right|_{\xi=1} = -1. \tag{29}$$

When one of the arguments is on the surface, i.e. $\boldsymbol{\xi}' = \mathbf{n}'$ ($\xi' = 1$), (28) simplifies into

$$\mathcal{G}^{(0)}(\boldsymbol{\xi}, \mathbf{n}') = \frac{2}{\sqrt{1 + \boldsymbol{\xi}^2 - 2(\boldsymbol{\xi} \cdot \mathbf{n}')}}$$
$$- \ln |1 - (\boldsymbol{\xi} \cdot \mathbf{n}') + \sqrt{1 + \boldsymbol{\xi}^2 - 2(\boldsymbol{\xi} \cdot \mathbf{n}')}|. \tag{30}$$

Note that, in general, because of the inhomogeneous boundary condition (29), the GF $\mathcal{G}^{(0)}(\boldsymbol{\xi}, \boldsymbol{\xi}')$ looses its symmetry of interchange $\boldsymbol{\xi} \longleftrightarrow \boldsymbol{\xi}'$. However, by imposing the condition $\oint_{\partial V} \mathcal{G}^{(0)}(\boldsymbol{\xi}, \mathbf{n}') d^2 n' = 0$, this symmetry is restored. The GF $\mathcal{G}^{(0)}(\boldsymbol{\xi}, \boldsymbol{\xi}')$ in (30) yields $(1/4\pi) \oint_{\partial V} \mathcal{G}^{(0)}(\boldsymbol{\xi}, \mathbf{n}') d^2 n' = 2 - \ln 2$, and hence by making the replacement $\mathcal{G}^{(0)} \to \mathcal{G}^{(0)} - (2 - \ln 2)$, which does not modify the boundary condition (29), we restore the symmetry $\boldsymbol{\xi} \longleftrightarrow \boldsymbol{\xi}'$.

For $\xi \ll 1$ (or $r \ll R$), we obtain the fourth-order expansion

$$\mathcal{G}^{(0)}(\boldsymbol{\xi}, \mathbf{n}) \simeq 2 - \ln 2 + 3(\mathbf{n} \cdot \boldsymbol{\xi}) + \frac{5}{4}[3(\mathbf{n} \cdot \boldsymbol{\xi})^2 - \xi^2]$$
$$+ \frac{7}{6}(\mathbf{n} \cdot \boldsymbol{\xi})[5(\mathbf{n} \cdot \boldsymbol{\xi})^2 - 3\xi^2]$$
$$+ \frac{9}{32}[35(\mathbf{n} \cdot \boldsymbol{\xi})^4 - 30(\mathbf{n} \cdot \boldsymbol{\xi})^2 \xi^2 + 3\xi^4] + \dots \tag{31}$$

In this section ($K_c = 0$), the spin deviation ψ_β is then given by [40]

$$\psi_\beta^{(0)}(\boldsymbol{\xi}) = \frac{1}{4\pi} \oint_{\partial V} d^2 n' \, \Sigma_\beta(\mathbf{m}_0, \mathbf{n}') \mathcal{G}^{(0)}(\boldsymbol{\xi}, \mathbf{n}'). \tag{32}$$

Note that had we kept the constant $2 - \ln 2$ in $\mathcal{G}^{(0)}(\boldsymbol{\xi}, \mathbf{n})$, we would have obtained the same result since the contribution of this constant term vanishes under the surface integral when we substitute Σ_β from equations (21) 18). For the same reason, odd-order terms in the expansion (31) do not contribute to (32).

Therefore, using (18) and the expansion (31) up to 4nd order in ξ, we obtain the following explicit expressions ($\xi = r/R$) for the components of the spin deviation vector $\boldsymbol{\psi}^{(0)}$:

$$\psi_1^{(0)} \simeq \lambda_s \frac{m_{0,x} m_{0,y}}{\sqrt{1 - m_{0,z}^2}} (\xi_x^2 - \xi_y^2) \left[1 + \frac{1}{16}(7\xi_z^2 - \xi^2) \right],$$

$$\psi_2^{(0)} \simeq \lambda_s \frac{m_{0,z}}{\sqrt{1 - m_{0,z}^2}} \left\{ \begin{array}{l} m_{0,x}^2(\xi_x^2 - \xi_z^2) + m_{0,y}^2(\xi_y^2 - \xi_z^2) + \\ \frac{1}{16}[m_{0,x}^2(\xi_x^2 - \xi_z^2)(7\xi_y^2 - \xi^2) + m_{0,y}^2(\xi_y^2 - \xi_z^2)(7\xi_x^2 - \xi^2)] \end{array} \right\}, \tag{33}$$

where $\lambda_s \equiv 15\widetilde{k}_s/32$. These expressions have been obtained using the following integrals

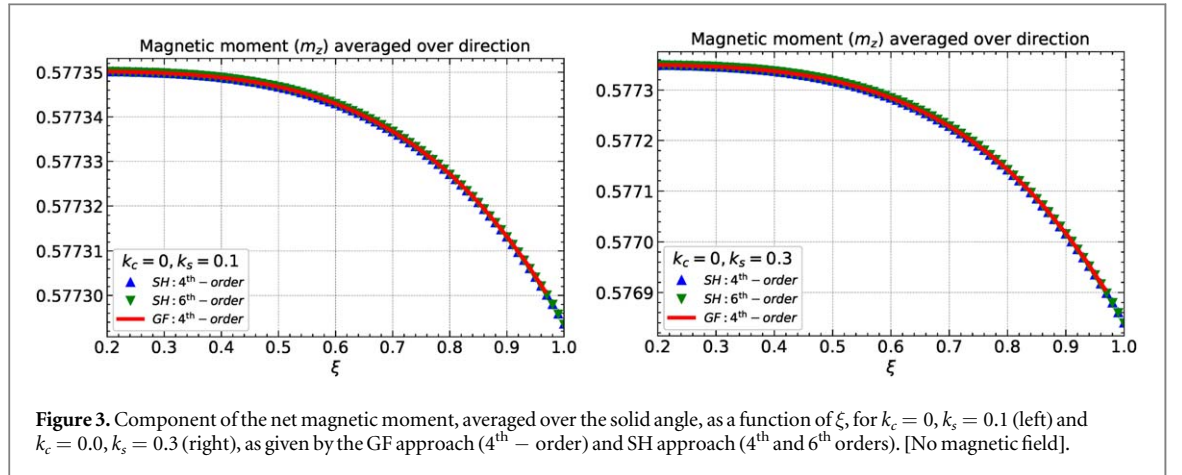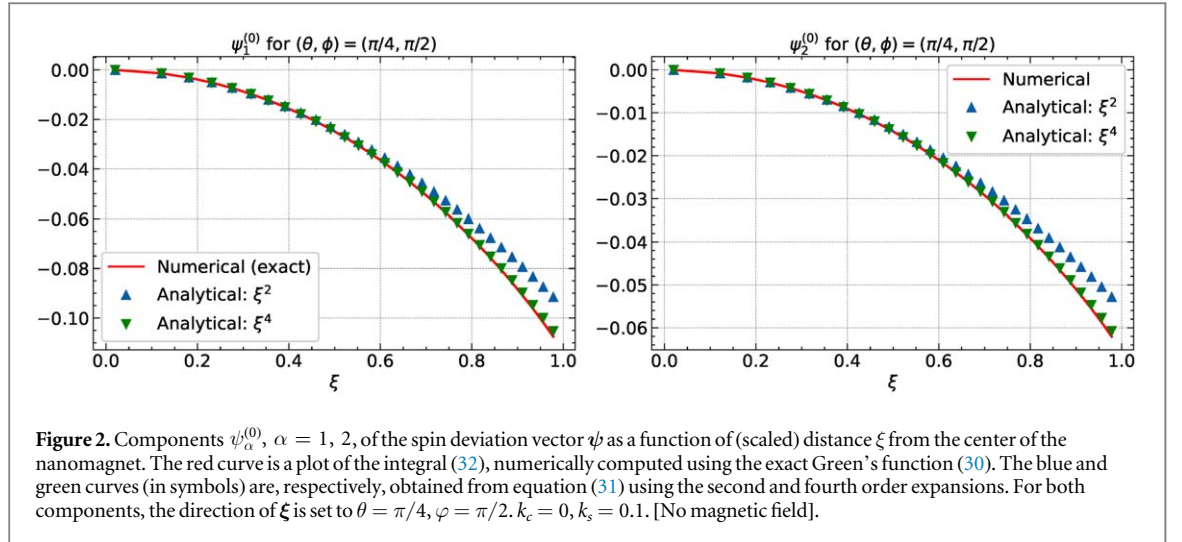$$\frac{3}{4\pi} \oint_{\partial V} (\mathbf{n} \cdot \boldsymbol{\xi}) |n_\alpha| \, d^2 n = 0, \quad \alpha = x, y, z,$$

$$\frac{1}{4\pi} \oint_{\partial V} [3(\mathbf{n} \cdot \boldsymbol{\xi})^2 - \xi^2] |n_\alpha| \, d^2 n = \frac{1}{8}(3\xi_\alpha^2 - \xi^2),$$

$$\frac{1}{4\pi} \oint_{\partial V} [35(\mathbf{n} \cdot \boldsymbol{\xi})^4 - 30(\mathbf{n} \cdot \boldsymbol{\xi})^2 \xi^2 + 3\xi^4] |n_\alpha| \, d^2 n = -\frac{1}{48}(35\xi_\alpha^4 - 30\xi^2 \xi_\alpha^2 + 3\xi^4). \tag{34}$$

We see in equation (33) that the spin deviation $\boldsymbol{\psi}^{(0)}$, caused by surface anisotropy, is linear in the corresponding constant k_s (through λ_s) and depends on the equilibrium magnetic moment $\mathbf{m}_0$. It is also clear that this deviation depends on the position within the NM and on the direction along which ξ is varied from the center out to the boundary of the NM. These results corroborate the discussion of the spin configuration shown in figure 1.

When $\mathbf{r}$ is on the surface, i.e. $\boldsymbol{\xi} = \mathbf{n}$, we obtain the largest deviation with respect to the homogeneous state $\mathbf{m}_0$ (using the ξ^2 expansion):

$$\psi_1^{(0)}(\mathbf{n}, \mathbf{m}_0) \simeq \lambda_s (n_x^2 - n_y^2) \frac{m_{0,x} m_{0,y}}{\sqrt{1 - m_{0,z}^2}},$$

$$\psi_2^{(0)}(\mathbf{n}, \mathbf{m}_0) \simeq \lambda_s \frac{m_{0,z}}{\sqrt{1 - m_{0,z}^2}} [(n_x^2 - n_z^2) m_{0,x}^2 + (n_y^2 - n_z^2) m_{0,y}^2]. \tag{35}$$

As we will see below and in the next section, it is handier in practice to use the expansions in equation (33) than the exact integral (32). For this purpose, we compare the two in figure 2.

Figure 2. Components $\psi_\alpha^{(0)}$, $\alpha = 1$, 2, of the spin deviation vector $\boldsymbol{\psi}$ as a function of (scaled) distance ξ from the center of the nanomagnet. The red curve is a plot of the integral (32), numerically computed using the exact Green's function (30). The blue and green curves (in symbols) are, respectively, obtained from equation (31) using the second and fourth order expansions. For both components, the direction of $\boldsymbol{\xi}$ is set to $\theta = \pi/4$, $\varphi = \pi/2$. $k_c = 0$, $k_s = 0.1$. [No magnetic field].

Figure 3. Component of the net magnetic moment, averaged over the solid angle, as a function of ξ, for $k_c = 0$, $k_s = 0.1$ (left) and $k_c = 0.0$, $k_s = 0.3$ (right), as given by the GF approach ($4^{\text{th}} -$ order) and SH approach (4th and 6th orders). [No magnetic field].

The plots in figure 2 show that the $4^{\text{th}} -$ order expansion of the Green function (30) renders a fairly good approximation to the components of $\boldsymbol{\psi}$ for all ξ between 0 and 1, i.e. from the center of the nanomagnet up to its border.

We have also compared these results, rendered by the Green's function technique, to the solution of the same boundary problem using the technique of spherical harmonics (SH), presented in [16, 17]. The outcome of this comparison is shown in figure 3 for two values of k_s. Note that here we have averaged the net magnetic moment over the direction solid angle [see discussion below]. We see that the $4^{\text{th}} -$ order approximation given in equation (31) and adopted here for the Green's function $\mathcal{G}^{(0)}(\mathbf{n}, \boldsymbol{\xi}')$, agrees very well with the expansion in terms of spherical harmonics up to the same order, to the 6th and even to the 10th order (not shown).

Next, using (14), we can now write explicit expressions for the components of the NM magnetic moment, m_α, $\alpha = x, y, z$. In the frame $(\mathbf{m}_0, \mathbf{u}_1, \mathbf{u}_2)$ with $\mathbf{u}_1$ and $\mathbf{u}_2$ given in equation (22), we have

$$\boldsymbol{\psi}(\mathbf{r}) = \psi_1 \mathbf{u}_1 + \psi_2 \mathbf{u}_2$$

or using $m_{0,\alpha} = 1/\sqrt{3}$ and

$$\mathbf{u}_1 \cdot \mathbf{e}_x = \frac{1}{\sqrt{2}}, \ \mathbf{u}_1 \cdot \mathbf{e}_y = \frac{-1}{\sqrt{2}}, \ \mathbf{u}_1 \cdot \mathbf{e}_z = 0,$$

$$\mathbf{u}_2 \cdot \mathbf{e}_x = \frac{1}{\sqrt{6}}, \ \mathbf{u}_2 \cdot \mathbf{e}_y = \frac{1}{\sqrt{6}}, \ \mathbf{u}_2 \cdot \mathbf{e}_z = -\sqrt{\frac{2}{3}},$$

we write $\psi(\mathbf{r})$ in the frame $(\mathbf{e}_x,\ \mathbf{e}_y,\ \mathbf{e}_z)$ as:

$$\psi(\mathbf{r}) = \psi_x \mathbf{e}_x + \psi_y \mathbf{e}_y + \psi_z \mathbf{e}_z = \frac{1}{\sqrt{2}} \begin{pmatrix} \psi_1 + \dfrac{1}{\sqrt{3}}\psi_2 \\[4pt] -\psi_1 + \dfrac{1}{\sqrt{3}}\psi_2 \\[4pt] -\dfrac{2}{\sqrt{3}}\psi_2 \end{pmatrix}.$$

Therefore, to 2nd order in r (or ξ), we obtain the spatial profile of the net magnetic moment (for $k_c = 0$)

$$\mathbf{m}(\mathbf{r}) \cong \mathbf{m}_0 + \psi(\mathbf{r}) = \begin{pmatrix} \dfrac{1}{\sqrt{3}} + \dfrac{1}{\sqrt{2}}\left(\psi_1^{(0)} + \dfrac{1}{\sqrt{3}}\psi_2^{(0)}\right) \\[10pt] \dfrac{1}{\sqrt{3}} + \dfrac{1}{\sqrt{2}}\left(-\psi_1^{(0)} + \dfrac{1}{\sqrt{3}}\psi_2^{(0)}\right) \\[10pt] \dfrac{1}{\sqrt{3}}(1 - \sqrt{2}\,\psi_2^{(0)}) \end{pmatrix}$$

with

$$\psi_1^{(0)} = \frac{\lambda_s}{R^2}\frac{1}{\sqrt{6}}(\tilde{\xi}_x^2 - \tilde{\xi}_y^2)r^2,$$

$$\psi_2^{(0)} = \frac{\lambda_s}{R^2}\frac{1}{3\sqrt{2}} \times [(\tilde{\xi}_x^2 - \tilde{\xi}_z^2) + (\tilde{\xi}_y^2 - \tilde{\xi}_z^2)]r^2$$

where $\tilde{\boldsymbol{\xi}} \equiv \boldsymbol{\xi}/\xi = (\sin\theta\cos\varphi,\ \sin\theta\sin\varphi,\ \cos\theta)$ gives the direction of $\boldsymbol{\xi}$ within the nanomagnet.

More explicitly, we have

$$\mathbf{m}(\xi, \theta, \varphi) \cong \mathbf{m}_0 + \frac{\lambda_s}{3\sqrt{12}} \begin{pmatrix} \sin^2\theta(1 + 3\cos 2\varphi) - 2\cos^2\theta \\ \sin^2\theta(1 - 3\cos 2\varphi) - 2\cos^2\theta \\ -2(\sin^2\theta - 2\cos^2\theta) \end{pmatrix} \xi^2. \tag{36}$$

This analytical result, a quadratic expansion in ξ, may be compared to the numerical solution of the LLE (4). However, such a comparison is not easy in practice and here is why.

The magnetization profile similar to equation (36) has been obtained, in the discrete approach, by solving the (damped) LLE (4) for a spherical NM as defined earlier with the Hamiltonian in equation (1). More precisely, we prepare the NM by cutting a sphere in a simple-cubic 3D lattice of linear size $N = N_x = N_y = N_z$, the outcome being a sphere-shaped ensemble of $\mathcal{N}$ spins. Then, we set the physical parameters J, K_c, K_s, h, etc, and run the Heun (or 4th-order Runge-Kutta) routine to solve equation (4), until the equilibrium state is reached. The result is a spin configuration similar to that shown in figure 1. For each such a spin configuration, we collect the spatial profile of the net magnetic moment $\mathbf{m}$ as we go from the center to the border of the NM, in a given direction. Now, because of the discreteness of the underlying lattice (inside a spherical NM cut out of a simple-cubic lattice), the raw profile, or the components of $\mathbf{m}$ in equation (3) as a function of the lattice site $\mathbf{r}_i$, yields rather jagged plots. In order to smooth out the data, we may average over the direction $(\theta,\ \varphi)$ of $\boldsymbol{\xi}$ and consider only the radial profile of $\mathbf{m}$, i.e. $\mathbf{m}(\xi)$. This is given by

$$\langle \mathbf{m}\rangle_\Omega = \oint_{\partial V} \frac{d\Omega}{4\pi}\, \mathbf{m}(\boldsymbol{\xi}) = \mathbf{m}_0 \times \left[1 - \frac{1}{2}\oint_{\partial V}\frac{d\Omega}{4\pi}\|\psi(\mathbf{r})\|^2\right]. \tag{37}$$
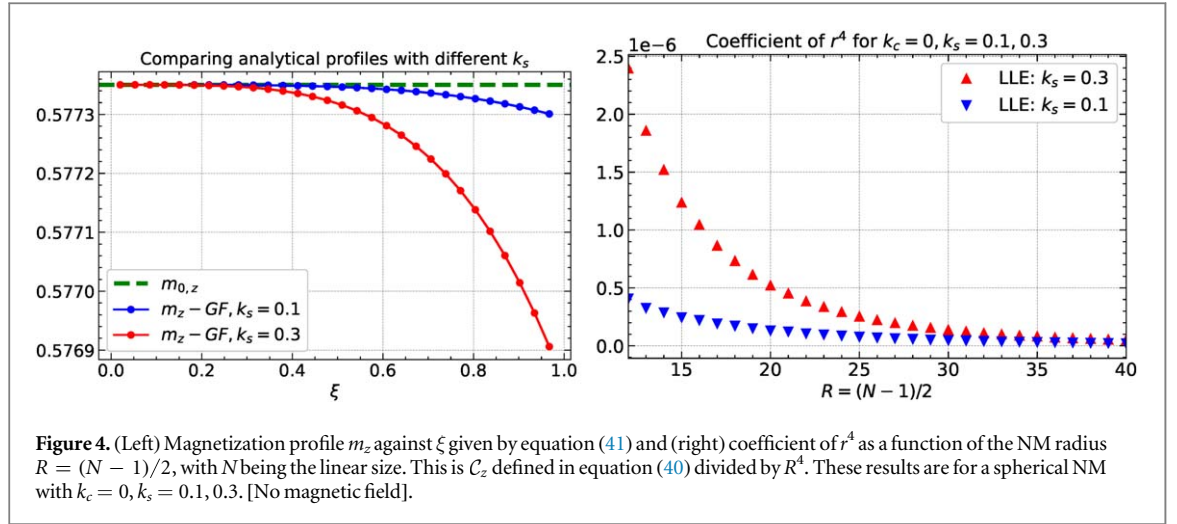
We see that upon averaging over the direction $(\theta,\ \varphi)$, the linear contribution in ψ vanishes. This can also be checked by performing the same average in equation (32) which, in turn, amounts to checking that the average of the GF (30) over the direction of $\boldsymbol{\xi}$ vanishes. This result is consistent with and justifies the condition (13).

Then, the integration over Ω yields

$$\oint_{\partial V} \frac{d\Omega}{4\pi}(\tilde{\xi}_\alpha^2 - \tilde{\xi}_\beta^2)^2 = \frac{4}{15}, \qquad \oint_{\partial V}\frac{d\Omega}{4\pi}(\tilde{\xi}_x^2 - \tilde{\xi}_z^2)(\tilde{\xi}_y^2 - \tilde{\xi}_z^2) = \frac{2}{15}$$

and upon using $1 = (m_{0,z}^2 + m_{0,x}^2 + m_{0,y}^2)^2$, we obtain

$$\oint_{\partial V}\frac{d\Omega}{4\pi}\|\psi(\mathbf{r})\|^2 = \frac{2}{15}\lambda_s^2\left(1 - \sum_\alpha m_{0,\alpha}^4\right)\xi^4. \tag{38}$$

Figure 4. (Left) Magnetization profile m_z against ξ given by equation (41) and (right) coefficient of r^4 as a function of the NM radius $R = (N - 1)/2$, with N being the linear size. This is $\mathcal{C}_z$ defined in equation (40) divided by R^4. These results are for a spherical NM with $k_c = 0$, $k_s = 0.1, 0.3$. [No magnetic field].

This finally leads to the solid-angle average of the magnetization profile

$$\langle \mathbf{m} \rangle_\Omega(\xi) \simeq \mathbf{m}_0 \left[1 - \frac{\lambda_s^2}{15} \left(1 - \sum_\alpha m_{0,\alpha}^4 \right) \xi^4 \right]. \tag{39}$$

Note that upon averaging over the direction (θ, φ), the quadratic contribution in equation (36) vanishes and only the quartic contribution remains in the expansion (14). The experimental techniques at our disposal today are not precise enough to allow for a probe of the magnetization profile in a given direction (θ, φ) within the nanomagnet. In addition, even if this were possible, the prototypical nanomagnet samples are assemblies with distributed nanomagnets and, as such only an average over the whole assembly can be accessed by measurements. This implies that if we were able to probe the magnetization profile, we should most likely observe the quartic behavior given by equation (39).

For later reference, we introduce the coefficient (of ξ^4)

$$\mathcal{C}_\beta \equiv m_{0,\beta} \frac{\lambda_s^2}{15} \left(1 - \sum_\alpha m_{0,\alpha}^4 \right), \quad \beta = x, y, z. \tag{40}$$

In order to further smooth out the lattice-induced jaggedness of the numerical data, we may also average over the magnitude of ξ taken within slices (or ring bands) perpendicular to the radial direction. For this, we adopt an onion structure for the NM and plot the net magnetic moment $\langle \mathbf{m} \rangle_\Omega$ as a function of the points ξ_n, $i = 1 \ldots M$, each of which being the center of a ring band. Doing so, leads to the discrete expression

$$\langle \mathbf{m} \rangle_\Omega^n(\xi_n) \simeq \mathbf{m}_0 - \mathbf{m}_0 \frac{\lambda_s^2}{15} \left(1 - \sum_\alpha m_{0,\alpha}^4 \right) \xi_n^4$$
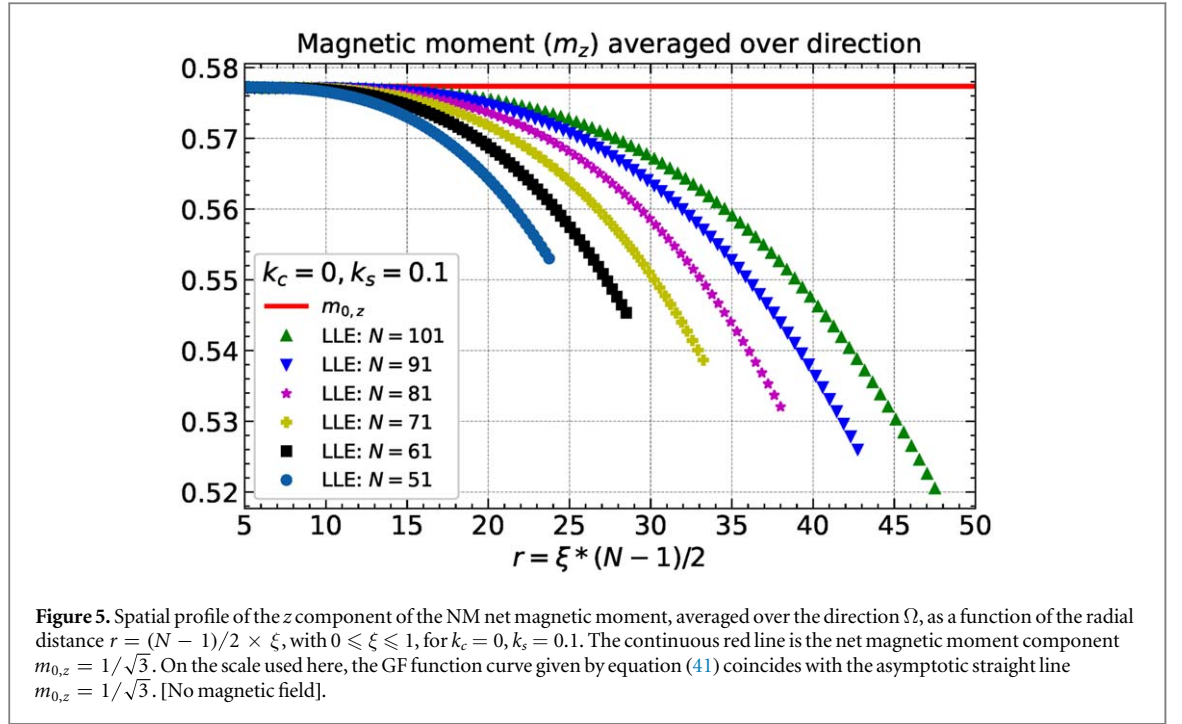
or component-wise

$$\langle m_\beta \rangle_\Omega^n(\xi_n) \simeq m_{0,\beta} - \mathcal{C}_\beta \xi_n^4. \tag{41}$$

In the numerical calculations (numerical solution of the LLE), from each spin configuration obtained for a set of physical parameters and a given linear size N, we infer the average $\langle \mathbf{m} \rangle_\Omega^n(r_n = R\xi_n)$. The latter is fit to $a_\beta - \mathcal{C}_\beta r^4$, for $\beta = x, y, z$, to obtain the coefficient $\mathcal{C}_\beta$. The results are shown in figure 4 (right). It is clearly seen that a larger k_s corresponds to a larger coefficient and thereby to stronger spin misalignments or deviations from $\mathbf{m}_0$. In addition, as the radius of the NM increases (we only show part of the data that have been obtained for $N = 25, 26, \ldots, 111$ or $R = 12, 13, \ldots, 55$), the coefficients for different values of k_s tend to zero. Indeed, as the size increases, the ratio of the number of surface spins to the total number decreases to zero. This translates into negligible surface effects and thereby to vanishing spin deviations. Indeed, a fit of the curves in figure 4 (right) yields $\mathcal{C}_\beta \sim R^{-2}$, leading to $\langle m_\beta \rangle_\Omega^n(r) \sim a_\beta - (b_\beta/R^2) r^4$, where b_β is a constant. This is illustrated in figure 5 where we compare the magnetic profile for different sizes to $m_{0,z}$, the magnetic moment in the uniform state. Finally, it is worth noting, by examining the vertical scale, that the deviation of the magnetic moment from the net direction $\mathbf{m}_0$ is rather small but it increases towards the NM boundary.

3.2. In the presence of core anisotropy

The more realistic situation with anisotropy in the core of the NM ($K_c \neq 0$), as well as on the surface ($K_s \neq 0$), is more involved. Indeed, there is no GF solving the problem stated in equations (24) 25). However, since the

Figure 5. Spatial profile of the *z* component of the NM net magnetic moment, averaged over the direction Ω, as a function of the radial distance $r = (N-1)/2 \times \xi$, with $0 \leqslant \xi \leqslant 1$, for $k_c = 0, k_s = 0.1$. The continuous red line is the net magnetic moment component $m_{0,z} = 1/\sqrt{3}$. On the scale used here, the GF function curve given by equation (41) coincides with the asymptotic straight line $m_{0,z} = 1/\sqrt{3}$. [No magnetic field].

coefficients κ_α^2 in equation (19) are small, owing to the fact that the core anisotropy and the applied field are, in typical situations, small with respect to the exchange coupling, we can use a perturbative approach. Indeed, we may write [30]

$$\psi_\beta(\xi) \simeq \psi_\beta^{(0)}(\xi) + \kappa_\beta^2 \psi_\beta^{(1)}(\xi). \tag{42}$$

Then, substituting in equation (17), using $\Delta_\xi \psi_\beta^{(0)}(\xi) = 0$ [see section 3.1] and dropping the term in κ_β^4, leads to

$$\Delta_\xi \psi_\beta^{(1)}(\xi) = \psi_\beta^{(0)}(\xi).$$

Next, we have

$$\left.\frac{d\psi_\beta}{d\xi}\right|_{\xi=1} = \left.\frac{d\psi_\beta^{(0)}}{d\xi}\right|_{\xi=1} + \kappa_\beta^2 \left.\frac{d\psi_\beta^{(1)}}{d\xi}\right|_{\xi=1}.$$

Now, $\psi^{(0)}$ is the major contribution to ψ that stems from surface anisotropy and $\psi^{(1)}$ appears only in the presence of core anisotropy and/or applied magnetic field ($\kappa_\beta \neq 0$), which tend to reduce the spin misalignments. We may then consider that $\psi^{(0)}$ still satisfies the boundary conditions (18), thus leading to

$$\left.\frac{d\psi_\beta^{(1)}}{d\xi}\right|_{\xi=1} = 0.$$

Therefore, $\psi_\beta^{(1)}$ is a field that satisfies Poisson's equation subjected to homogeneous Neumann boundary conditions, namely

$$\Delta_\xi \psi_\beta^{(1)}(\xi) = \psi_\beta^{(0)}(\xi), \tag{43}$$

$$\left.\frac{d\psi_\beta^{(1)}}{d\xi}\right|_{\xi=1} = 0. \tag{44}$$

The solution of this problem can only exist if $\int_V d\xi \, \psi_\beta^{(0)}(\xi) = 0$. It can be checked that this is indeed the case by using expressions (33). This is also compatible with the condition (13) that could be assumed to apply at all orders of perturbation. In this case, there exists a GF, call it $\tilde{\mathcal{G}}(\xi', \xi)$, satisfying

$$\begin{cases} \Delta_\xi \tilde{\mathcal{G}}(\boldsymbol{\xi}', \boldsymbol{\xi}) = -4\pi\delta(\boldsymbol{\xi} - \boldsymbol{\xi}'), \\ \dfrac{d\tilde{\mathcal{G}}(\boldsymbol{\xi}', \boldsymbol{\xi})}{d\xi}\bigg|_{\xi=1} = -1. \end{cases} \tag{45}$$

The solution of the problem then reads [40]

$$\psi_\beta^{(1)}(\boldsymbol{\xi}) = -\frac{1}{4\pi}\int_V d\boldsymbol{\xi}'\,\tilde{\mathcal{G}}(\boldsymbol{\xi}', \boldsymbol{\xi})\psi_\beta^{(0)}(\boldsymbol{\xi}') - \frac{1}{4\pi}\oint_{\partial V} d^2n'\,\psi_\beta^{(1)}(\mathbf{n}')\frac{d\tilde{\mathcal{G}}(\boldsymbol{\xi}', \boldsymbol{\xi})}{d\xi'}\bigg|_{\xi'=1}$$

$$= -\frac{1}{4\pi}\int_V d\boldsymbol{\xi}'\,\tilde{\mathcal{G}}(\boldsymbol{\xi}', \boldsymbol{\xi})\psi_\beta^{(0)}(\boldsymbol{\xi}') + D_\beta,$$

where D_β is a constant. In fact, we see that $\tilde{\mathcal{G}}(\boldsymbol{\xi}, \boldsymbol{\xi}')$ is the solution of the same problem as $\mathcal{G}^{(0)}(\boldsymbol{\xi}, \boldsymbol{\xi}')$ and, as such, we may simply take $\tilde{\mathcal{G}}(\boldsymbol{\xi}, \boldsymbol{\xi}') = \mathcal{G}^{(0)}(\boldsymbol{\xi}, \boldsymbol{\xi}')$. In addition, the constant D_β can be determined by assuming that the spin mis-alignment vanishes at the center of the NM, i.e. $\psi_\beta^{(1)}(\mathbf{0}) = 0$. This yields, using equation (28), $D_\beta = \frac{1}{4\pi}\int_V d\boldsymbol{\xi}\,\mathcal{G}^{(0)}(0, \boldsymbol{\xi})\psi_\beta^{(0)}(\boldsymbol{\xi}) = 0$.

Finally, we obtain the solution

$$\psi_\beta^{(1)}(\boldsymbol{\xi}) = -\frac{1}{4\pi}\int_V d\boldsymbol{\xi}'\,\mathcal{G}^{(0)}(\boldsymbol{\xi}, \boldsymbol{\xi}')\psi_\beta^{(0)}(\boldsymbol{\xi}'). \tag{46}$$

Note that this result can also be obtained by proceeding through an expansion of the GF $\mathcal{G}_\beta(\boldsymbol{\xi}, \mathbf{n}')$ that appears in equation (24), instead of the expansion in equation (42). This is done in appendix. Equation (46), which derives from equation (43), suggests that $\psi_\beta^{(0)}$ acts as a source for the field $\psi_\beta^{(1)}$.

Let us now discuss the explicit calculation of the components $\psi_\beta^{(1)}(\boldsymbol{\xi})$ of the spin deviation. Note that in equation (46), we have an integral over the volume and thereby none of the arguments of $\mathcal{G}^{(0)}(\boldsymbol{\xi}, \boldsymbol{\xi}')$ is fixed on the surface. As a consequence, we have to use the exact expression (28), instead of the expansion (31). Unfortunately, it is then difficult to obtain a closed analytical result for the integral in equation (46). On the other hand, if we use instead the representation (46) in terms of the GF $\mathcal{G}^{(1)}$ in equation (A3), we again encounter an integral over the volume of the product of two $\mathcal{G}^{(0)}$, one of which has both arguments inside ∂V. Consequently, we can provide analytical (approximate) expressions for $\psi_\beta^{(1)}(\boldsymbol{\xi})$ only for $\boldsymbol{\xi}$ on the boundary ∂V. This should yield the largest contribution from $\psi_\beta^{(1)}(\boldsymbol{\xi})$, as one obtains for $\psi_\beta^{(0)}$ in equation (35), see below. For arbitrary $\boldsymbol{\xi}$, with $0 \leqslant \xi \leqslant 1$, we must resort to numerical integration.

For $\boldsymbol{\xi}$ on the boundary ∂V, *i.e.* $\boldsymbol{\xi} = \mathbf{n}$, we use equations (31) and (35) to derive the following expressions for the components of $\boldsymbol{\psi}^{(1)}$ on the sphere:

$$\psi_1^{(1)}(\mathbf{n}, \mathbf{m}_0) \simeq -\frac{\lambda_s}{14}\frac{m_{0,x}m_{0,y}}{\sqrt{1 - m_{0,z}^2}}(n_y^2 - n_x^2),$$

$$\psi_2^{(1)}(\mathbf{n}, \mathbf{m}_0) \simeq -\frac{\lambda_s}{14}\frac{m_{0,z}}{\sqrt{1 - m_{0,z}^2}}[(n_x^2 - n_z^2)m_{0,x}^2 + (n_y^2 - n_z^2)m_{0,y}^2]. \tag{47}$$

The components of the largest spin deviation represented by the (total) vector $\boldsymbol{\psi}$, within a spherical NM with equilibrium magnetic moment $\mathbf{m}_0$, are obtained by substituting (35) and (47) into equation (42). This yields

$$\psi_1(\mathbf{n}, \mathbf{m}_0) \simeq \lambda_s\left(1 - \frac{\kappa_1^2}{14}\right)\frac{m_{0,x}m_{0,y}}{\sqrt{1 - m_{0,z}^2}}(n_x^2 - n_y^2),$$

$$\psi_2(\mathbf{n}, \mathbf{m}_0) \simeq \lambda_s\left(1 - \frac{\kappa_2^2}{14}\right)\frac{m_{0,z}}{\sqrt{1 - m_{0,z}^2}}[(n_x^2 - n_z^2)m_{0,x}^2 + (n_y^2 - n_z^2)m_{0,y}^2]. \tag{48}$$

Note that because of the factor $1 - \kappa_\alpha^2/14$, these expressions are valid for $\kappa_\alpha \leqslant \sqrt{14} \simeq 3.74$. However, since they have been derived using an expansion in κ_α, these expressions are actually valid for a much smaller κ_α and the previous condition adds no new constraint.

We can also numerically compute the integral in (46) and then average over the solid angle. However, although this procedure is quite affordable to today's computers using optimized algorithms, it still remains rather costly with regard to the CPU resources, especially when several curves are needed for comparison. Here, we resort to the numerical solution of the LLE system, as done in the case of $k_c = 0$, which allows for the full procedure in an easier manner. Accordingly, in figure 6 we plot the deviation of the z component of the net magnetic moment, $\delta m_z \equiv m_z(r) - m_z(0)$, averaged over the direction Ω, as a function of the radial distance $r = (N - 1)/2 \times \xi$, for $k_s = 0.3$ and $k_c = 0.01$ (full lines) and $k_c = 0$ (dashed lines). We recall that the uniaxial anisotropy here is taken along the z axis. If it is taken along the cube diagonal, the deviations will be much smaller. Indeed, we note that in the presence of anisotropy in the core with an easy axis in the z direction, the
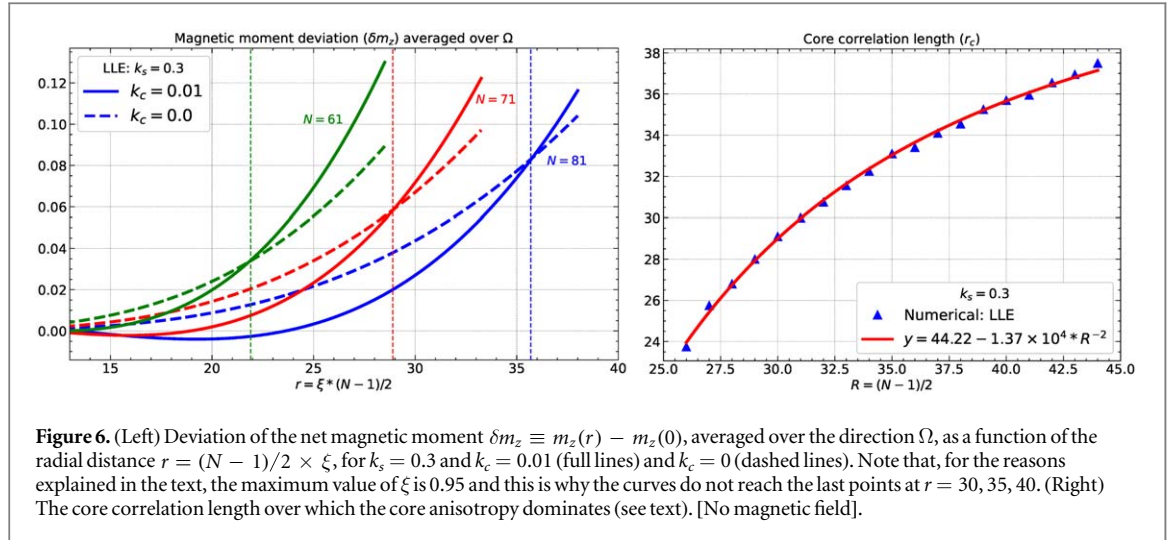
Figure 6. (Left) Deviation of the net magnetic moment $\delta m_z \equiv m_z(r) - m_z(0)$, averaged over the direction Ω, as a function of the radial distance $r = (N-1)/2 \times \xi$, for $k_s = 0.3$ and $k_c = 0.01$ (full lines) and $k_c = 0$ (dashed lines). Note that, for the reasons explained in the text, the maximum value of ξ is 0.95 and this is why the curves do not reach the last points at $r = 30, 35, 40$. (Right) The core correlation length over which the core anisotropy dominates (see text). [No magnetic field].

state $\mathbf{m}_0$ is no longer along the cube diagonal; it is tilted towards the z axis by an angle that depends on the relative strength of the core anisotropy (k_c). This results in a competition between the core and surface anisotropies.

The results in figure 6 show that, both with and without core anisotropy, the overall spin deviations are reduced when the NM size increases. In addition, here we see that for a given size N of the NM, the curves with and without core anisotropy (same color) intersect at a given distance r_c from the center of the NM. As discussed earlier, the spin misalignments induced by the surface anisotropy tend to propagate from the boundary to the center of the NM, while the effect of the core (uniaxial) anisotropy is to align the spins parallel to each other and thus to push the spin misalignments out to the border. The competition between these two effects results in a critical radius r_c, or core correlation length (indicated by the dashed vertical lines), over which the core anisotropy dominates, thereby rendering a weaker spin deviation. This is illustrated by the fact that, for $r \leqslant r_c$, the continuous curves ($k_c \neq 0$) are below the dashed ones ($k_c = 0$). Furthermore, in the plot on the right, we see that the distance r_c increases with the radius $R = (N-1)/2$ of the NM; it behaves as $a - b/R^2$ with $b > 0$ (see the fitting curve in red). So, as R increases the surface relative contribution decreases and the core anisotropy then dominates and pushes the spin noncollinearities farther out towards the NM border. As a consequence, the surface contribution to the overall anisotropy of the NM scales with the surface ($\sim R^2$), as was discussed in [27].

4. Summary, Conclusions, and Outlook

We have built a formalism for solving the Helmholtz equation, with inhomogeneous Neumann boundary conditions, satisfied by the spin deviation vector induced by surface anisotropy in a nanomagnet, using the technique of Green's functions in the continuum limit. The nanomagnet has been modeled as a spherical crystallite of $\mathcal{N}$ atomic magnetic moments and whose energy comprises the exchange interaction, the Zeeman contribution and the anisotropy energy that discriminates between spins in the core, attributed a uniaxial anisotropy, and spins at the surface whose anisotropy is given by Néel's model. We have also provided the numerical solution of a system of coupled Landau–Lifshitz equations written for the atomic magnetic moments and compared the results to those of the analytical approach. We have computed the solid-angle averaged components of the nanomagnet's net moment as a function of the distance to the NM center in the radial direction, both in the absence and presence of anisotropy in the core. In the former case, we have provided good approximate analytical expressions for the spin deviation at an arbitrary position within the nanomagnet. In the latter case, however, the solution is only given numerically, either through a volume integral within the Green's function approach, or numerically by solving the Landau–Lifshitz equations. Nonetheless, an analytical solution for this case has been given on the boundary of the NM, which represents the largest spin deviation. Both the numerical and (semi-)analytical results show that the spin deviations induced by surface anisotropy are stronger with larger surface anisotropy constant and/or smaller sizes.

As discussed in the introduction, the small-angle neutron scattering technique should provide us with a relatively precise probe of a signature of spin deviations in nanomagnets. However, with real samples, we are faced with various distributions (size, shape and anisotropy) and collective effects due to inter-particle interactions which may lead to a smearing out of the surface effects and the entailed sought-for spin misalignments. As a first step, we may consider doing measurements on an array of well separated platelets (or thin cylinders), thus avoiding strong inter-particle interactions while ensuring enhanced surface contributions

to the overall anisotropy. In parallel to these investigations, further theoretical endeavor is required in order to take account of the inter-particle interactions together with other forms of anisotropy that might stem from different shapes and internal structures of the nanomagnets (e.g. platelets). In this context, the present Green's function methodology may form the basis for computing the magnetic small angle neutron scattering cross-section of nanomagnets according to their magnetic materials parameters.

Acknowledgments

Data availability statement

All data that support the findings of this study are included within the article (and any supplementary files).

Conflicts of Interest

We confirm that our work presents no conflict of interest, as we have no financial, personal, or professional relationships that may interfere with the impartiality of our work or the validity of its findings.

Data access

Ethics statement

This work is a mathematical physics work that presents no ethical issues whatsoever.

Appendix. Expansion of the Green's function in the presence of core anisotropy

Similarly to the expansion of ψ in equation (42), we may write the GF $\mathcal{G}_\beta$ that appears in equation (24) as follows [30]

$$\mathcal{G}_\alpha(\mathbf{m}_0, \boldsymbol{\xi}, \boldsymbol{\xi}') = \mathcal{G}^{(0)}(\boldsymbol{\xi}, \boldsymbol{\xi}') + \kappa_\alpha^2(\mathbf{m}_0, \mathbf{h})\mathcal{G}^{(1)}(\boldsymbol{\xi}, \boldsymbol{\xi}') + \ldots. \tag{A1}$$

It is then easy to see, upon using equation (27), that the correction term $\mathcal{G}^{(1)}(\boldsymbol{\xi}, \boldsymbol{\xi}')$ satisfies the following equation (upon dropping terms in κ_α^4)

$$\Delta \mathcal{G}^{(1)}(\boldsymbol{\xi}, \boldsymbol{\xi}') \simeq \mathcal{G}^{(0)}(\boldsymbol{\xi}, \boldsymbol{\xi}') \tag{A2}$$

and that its solution can be written as a convolution

$$\mathcal{G}^{(1)}(\boldsymbol{\xi}, \boldsymbol{\xi}') = -\frac{1}{4\pi} \int_V \mathcal{G}^{(0)}(\boldsymbol{\xi}'', \boldsymbol{\xi}')\mathcal{G}^{(0)}(\boldsymbol{\xi}, \boldsymbol{\xi}') d^3\xi' \tag{A3}$$

with the boundary condition [using equation (29)]

$$\left.\frac{d\mathcal{G}^{(1)}}{d\xi}\right|_{\xi=1} = \frac{1}{4\pi} \int_V \mathcal{G}^{(0)}(\boldsymbol{\xi}'', \boldsymbol{\xi}')d^3\xi''. \tag{A4}$$

Then, in equation (26), we substitute the expansions for $\psi_\beta(\boldsymbol{\xi})$ and $\mathcal{G}_\beta(\boldsymbol{\xi}, \mathbf{n}')$, from equations (42) and (A1), respectively, and identifying the terms of the same order in κ_β, we obtain the following two equations

$$\psi_\beta^{(0)}(\boldsymbol{\xi}) = \frac{1}{4\pi} \oint_{\partial V} d^2 n' \left.\frac{d\psi_\beta}{d\xi}\right|_{\boldsymbol{\xi}=\mathbf{n}'} \mathcal{G}^{(0)}(\boldsymbol{\xi}, \mathbf{n}')$$

$$\psi_\beta^{(1)}(\boldsymbol{\xi}) = \frac{1}{4\pi} \oint_{\partial V} d^2 n' \left.\frac{d\psi_\beta}{d\xi}\right|_{\boldsymbol{\xi}=\mathbf{n}'} \mathcal{G}^{(1)}(\boldsymbol{\xi}, \mathbf{n}').$$

Next, using (44) we recover equation (32) for the component $\psi_\beta^{(0)}$ together with the following equation for $\psi_\beta^{(1)}$:

$$\psi_\beta^{(1)}(\boldsymbol{\xi}) = \frac{1}{4\pi} \oint_{\partial V} d^2 n' \Sigma_\beta(\mathbf{m}_0, \mathbf{n}') \mathcal{G}^{(1)}(\boldsymbol{\xi}, \mathbf{n}'). \tag{A5}$$

Then, replacing $\mathcal{G}^{(1)}(\boldsymbol{\xi}, \mathbf{n}')$ by its expression in equation (A3) leads to

$$\psi_\beta^{(1)}(\boldsymbol{\xi}) = -\frac{1}{4\pi} \int_V d^3\xi' \, \mathcal{G}^{(0)}(\boldsymbol{\xi}, \boldsymbol{\xi}') \left[\frac{1}{4\pi} \oint_{\partial V} d^2 n' \, \Sigma_\beta(\mathbf{m}_0, \mathbf{n}') \mathcal{G}^{(0)}(\boldsymbol{\xi}', \mathbf{n}') \right].$$

Here, we recognize the term between brackets as $\psi_\beta^{(0)}$, according to equation (32), thus recovering (up to a constant) the result obtained in equation (46). Note that the main difference between the two representations, is that (46) is an integral over the volume of the NM whereas (A5) is an integral over its surface.

References

[1] Huffman D R and Bohren C F 1983 *Absorption and Scattering of Light by Small Nanoparticles* (Willey-VCH Verlag GmbH)
[2] Jin *et al* 2003 Controlling anisotropic nanoparticle growth through plasmon excitation *Nature* **425** 487–90
[3] Zhu *et al* 2008 Correlating the crystal structure of a thiol-protected au25 cluster and optical properties *J. Am. Chem. Soc.* **130** 5883–5
[4] Jin *et al* 2016 Atomically precise colloidal metal nanoclusters and nanoparticles: fundamentals and opportunities *Chem. Rev.* **116** 10346–413
[5] Néel L 1953 L'anisotropie superficielle des substances ferromagnétiques *Compt. Rend. Acad. Sci.* **237** 1468
[6] Bean C P and Livingston J D 1959 Superparamagnetism *J. Appl. Phys.* **30** S120
[7] Kachkachi H and Garanin D A 2005 Magnetic nanoparticles as many-spin systems *Surface Effects in Magnetic Nanoparticles* ed D Fiorani (Springer) p 75
[8] Srajer G *et al* 2006 Advances in nanomagnetism via x-ray techniques *J. Magn. Magn. Mater.* **307** 1
[9] Schmool D S and Kachkachi H 2016 *Ch One—Collective Effects in Assemblies of Magnetic Nanaparticles. vol 67 of Solid State Physics* (Academic Press) pp 1–101
[10] Koumpouras K 2017 Atomistic spin dynamics and relativistic effects in chiral anomagnets *Thesis/Dissertation* Uppsala University
[11] Iglesias Ò and Kachkachi H 2021 *Single Nanomagnet Behaviour: Surface and Finite-Size Effects* (Springer International Publishing) pp 3–38
[12] Hirohata *et al* 2020 Review on spintronics: Principles and device applications *J. Magn. Magn. Mater.* **509** 166711
[13] Déjardin P-M, Kachkachi H and Kalmykov Y 2008 Thermal and surface anisotropy effects on the magnetization reversal of a nanocluster *J. Phys. D* **41** 134004
[14] Vernay F, Sabsabi Z and Kachkachi H 2014 ac susceptibility of an assembly of nanomagnets: Combined effects of surface anisotropy and dipolar interactions *Phys. Rev. B* **90** 094416
[15] Mühlbauer S *et al* 2019 Magnetic small-angle neutron scattering *Rev. Mod. Phys.* **91** 015004
[16] Adams M P, Michels A and Kachkachi H 2022 Magnetic neutron scattering from spherical nanoparticles with néel surface anisotropy: analytical treatment *J. Appl. Cryst.* **55** 1475–87
[17] Adams M P, Michels A and Kachkachi H 2022 Magnetic neutron scattering from spherical nanoparticles with néel surface anisotropy: atomistic simulations *J. Appl. Cryst.* **55** 1488–99
[18] Dimitrov D A and Wysin 1994 Effects of surface anisotropy on hysteresis in fine magnetic particles *Phys. Rev.* **50** 3077 B
[19] Kodama R H and Berkovitz A E 1999 Atomic-scale magnetic modeling of oxide nanoparticles *Phys. Rev. B* **59** 6321
[20] Kachkachi H and Garanin D A 2001 Boundary and finite-size effects in small magnetic systems *Physica A Statistical Mechanics and its Applications* **300** 487–504
[21] Kachkachi H and Garanin D A 2001 Spin-wave theory for finite classical magnets and superparamagnetic relation *European Physical Journal* B **22** 291–300
[22] Iglesias O and Labarta A 2001 Finite-size and surface effects in maghemite nanoparticles: Monte Carlo simulations *Phys. Rev. B* **63** 184416
[23] Kachkachi H and Dimian M 2002 Hysteretic properties of a magnetic particle with strong surface anisotropy *Phys. Rev. B* **66** 174419
[24] Kazantseva N, Hinzke D, Nowak U, Chantrell R W, Atxitia U and Chubykalo-Fesenko O 2008 Towards multiscale modeling of magnetic materials: simulations of FePt *Phys. Rev. B* **77** 184428
[25] Evans R F L, Fan W J, Chureemart P, Ostler T A, Ellis M O A and Chantrell R W 2014 Atomistic spin model simulations of magnetic nanomaterials *J. Phys.: Condens. Mat.* **26** 103202
[26] Néel L 1954 Anisotropie magnétique superficielle et surstructures d'orientation *J. Phys. Radium* **15** 225
[27] Garanin D A and Kachkachi H 2003 Surface contribution to the anisotropy of magnetic nanoparticles *Phys. Rev. Lett.* **90** 065504
[28] Kachkachi H and Mahboub H 2004 Surface anisotropy in nanomagnets: Néel or Transverse? Surface anisotropy in nanomagnets: néel or Transverse ? *J. Magn. Magn. Mater.* **278** 334
[29] Kachkachi H and Bonet E 2006 Surface-induced cubic anisotropy in nanomagnets *Phys. Rev. B* **73** 224402
[30] Kachkachi H 2007 Effects of spin non-collinearities in magnetic nanoparticles *J. Magn. Magn. Mater.* **316** 248
[31] Skomski R and Coey J M D 1999 *Permanent Magnetism, Studies in Condensed Matter Physics* vol 1 (IOP Publishing)
[32] Urquhart K B, Heinrich B, Cochran J F, Arrott A S and Myrtle K 1988 Ferromagnetic resonance in ultrahigh vacuum of bcc Fe(001) films grown on Ag(001) *J. Appl. Phys.* **64** 5334
[33] Perzynski R and Raikher Y L 2005 *Surface Effects in Magnetic Nanoparticles* ed D Fiorani (Springer) 141
[34] Turov E A 1965 *Physical Properties of Magnetically Ordered Crystals* (Academic Press)
[35] Garanin D A 2018 Effective anisotropy due to the surface of magnetic nanoparticles *Phys. Rev. B* **98** 2018
[36] Polyakov A M 2009 Interaction of Goldstone particles in two dimensions. applications to ferromagnets and massive yang-mills fields *Phys. Rev.* **80** 014420 B
[37] Garanin D A and Kachkachi H 2009 Magnetization reversal via internal spin waves in magnetic nanoparticles *Phys. Rev. B* **80** 014420
[38] Duffy D G 2015 *Green�s Functions With Applications* (Chapman and Hall/CRC)
[39] Morse P M and Feshbach H 1954 *Am. J. Phys.* **22** 410
[40] Morse P M and Feshbach H 1953 *Methods of Theoretical Physics.* (McGraw-Hill)
[41] Sadybekov M A, Torebek B T and Turmetov B K 2016 *Eurasian Math. J.* **7** 100